Grid-Interactive Electric Vehicle and Building Coordination Using Coupled Distributed Control

Preprint

Dylan Wald,[1,2] Kathryn Johnson,[1,2] Christopher J. Bay,[2] Jennifer King,[2] and Rohit Chintala[2]

1 Colorado School of Mines
2 National Renewable Energy Laboratory

Presented at 2022 American Control Conference (ACC)
Atlanta, Georgia
June 8–10, 2022

NREL is a national laboratory of the U.S. Department of Energy
Office of Energy Efficiency & Renewable Energy
Operated by the Alliance for Sustainable Energy, LLC

This report is available at no cost from the National Renewable Energy Laboratory (NREL) at www.nrel.gov/publications.

Contract No. DE-AC36-08GO28308

Conference Paper
NREL/CP-5000-82071
July 2022

Grid-Interactive Electric Vehicle and Building Coordination Using Coupled Distributed Control

Preprint

Dylan Wald,[1,2] Kathryn Johnson,[1,2] Christopher J. Bay,[2] Jennifer King,[2] and Rohit Chintala[2]

1 Colorado School of Mines
2 National Renewable Energy Laboratory

Suggested Citation
Wald, Dylan, Kathryn Johnson, Christopher J. Bay, Jennifer King, and Rohit Chintala. 2022. *Grid-Interactive Electric Vehicle and Building Coordination Using Coupled Distributed Control: Preprint*. Golden, CO: National Renewable Energy Laboratory. NREL/CP-5000-82071. https://www.nrel.gov/docs/fy22osti/82071.pdf.

NREL is a national laboratory of the U.S. Department of Energy
Office of Energy Efficiency & Renewable Energy
Operated by the Alliance for Sustainable Energy, LLC

This report is available at no cost from the National Renewable Energy Laboratory (NREL) at www.nrel.gov/publications.

Contract No. DE-AC36-08GO28308

Conference Paper
NREL/CP-5000-82071
July 2022

National Renewable Energy Laboratory
15013 Denver West Parkway
Golden, CO 80401
303-275-3000 • www.nrel.gov

NOTICE

This work was authored in part by the National Renewable Energy Laboratory, operated by Alliance for Sustainable Energy, LLC, for the U.S. Department of Energy (DOE) under Contract No. DE-AC36-08GO28308. Funding provided by the U.S. Department of Energy Office of Energy Efficiency and Renewable Energy Wind Energy Technologies Office. The views expressed herein do not necessarily represent the views of the DOE or the U.S. Government. The U.S. Government retains and the publisher, by accepting the article for publication, acknowledges that the U.S. Government retains a nonexclusive, paid-up, irrevocable, worldwide license to publish or reproduce the published form of this work, or allow others to do so, for U.S. Government purposes.

Cover Photos by Dennis Schroeder: (clockwise, left to right) NREL 51934, NREL 45897, NREL 42160, NREL 45891, NREL 48097, NREL 46526.

NREL prints on paper that contains recycled content.

Grid-Interactive Electric Vehicle and Building Coordination Using Coupled Distributed Control

Dylan Wald[1,2], Kathryn Johnson[1,2], Christopher J. Bay[2], Jennifer King[2], and Rohit Chintala[2]

***Abstract*— As an increasing number of controllable devices are introduced onto the grid, they can individually provide ancillary services in support of grid stability. However, the goals of each device differ due to their type and individual objectives, causing instances where they may conflict. To reduce the chances of these devices contributing to grid instability, these devices must effectively communicate in a cooperative manner to both meet their own needs while providing services to the grid. Previous work demonstrates that the Network Lasso - ADMM - Limited Communication - DMPC (NALD) algorithm allows coordination between two subsystems that use different control algorithms (building and charging stations) to provide services to the grid and individually optimize their performance in a specific scenario. The ideal NALD algorithm should be generalized to allow plug-and-play capabilities across devices of differing characteristics. This paper takes a step toward achieving this generalization by updating the electric vehicle charging objective and redefining the communication scheme compared to prior work to generalize the coordination and, as a result, improve the performance of the NALD algorithm.**

I. INTRODUCTION

As an increasing number of smart devices and electricity sources are integrated into the grid, an introduction of new voltage fluctuations and bidirectional power flows can negatively impact the control and operation of the grid [1]. Autonomous energy grids (AEGs) aim to autonomously optimize the operation of the grid as a whole in real time to promote affordability, reliability, and resiliency [1], [2]. Reference [2] uses this idea, wherein a network of AEGs is controlled using a hierarchical, distributed method, allowing systemwide load balancing despite the different types of loads and generation in each AEG. This balancing is facilitated through increased flexibility, a byproduct of many controllable devices, along with ample sensor information [1]–[3]. The increased flexibility and controllability of devices on the grid of the future enables real-time response to grid demands, requiring advanced coordination across devices to meet those demands.

An example of new controllable devices that could affect the grid are electric vehicles (EVs). Total EV sales around the world are expected to reach 58% by 2040 [4], leading to an increase in charging infrastructure and electrical loads on the grid. This increase could become a problem if many EVs are simultaneously charging during times of peak load which may cause demand to exceed the capacity of the grid infrastructure, leading to grid instability.

A typical controls solution to this problem is load shifting, i.e. shifting EV charging loads to times when the demand is lower [5]. Successful load shifting in the form of valley-filling is described in [6] and [7]. Other literature, such as [8] and [9], use demand-side management (DSM) to drive the EV charging control. Last, [10] uses a hierarchical model predictive control (MPC) approach to shift the EV charging load based on owner needs, reducing complexity and communication. While [6]–[10] all use unique methods to control EV charging to minimize the impact of EV charging on the grid, none allow coordination between EVs and other controllable devices to provide ancillary services. As a result, this paper proposes a method to control EV charging while coordinating with another device to meet a global objective.

Buildings are another example of controllable grid-connected devices. According to [11], in 2014, buildings accounted for more than 76% of all electricity use and 40% of the greenhouse gas emissions in the United States. Consequently, significant efforts in advanced heating, ventilation, and air conditioning (HVAC) system control [12] have been made to improve the building efficiency.

MPC has been a leader in HVAC control in buildings due to its many advantages such as handling of multiple states and disturbances and use of constraints [12]. Some MPC methods for building control are described in [13]–[16]. The case study in [17] uses MPC to optimize building efficiency while maximizing occupant comfort as a function of worker productivity. Machine-learning approaches, such as reinforcement learning, are also starting to gain traction in building control. Due to nonlinear complexities in most building models, some purely data-driven approaches have been applied to learn the optimal control strategies without knowing the building dynamics, such as [18]. Likewise, [19] further advances the work in [20] by using an artificial neural network to learn the MPC control actions in [20],

*This work was authored in part by the National Renewable Energy Laboratory, operated by Alliance for Sustainable Energy, LLC, for the U.S. Department of Energy (DOE) under Contract No. DE-AC36–08GO28308. Funding provided by the U.S. Department of Energy Office of Energy Efficiency and Renewable Energy Wind Energy Technologies Office. The views expressed in the article do not necessarily represent the views of the DOE or the U.S. Government. The U.S. Government retains and the publisher, by accepting the article for publication, acknowledges that the U.S. Government retains a nonexclusive, paid-up, irrevocable, worldwide license to publish or reproduce the published form of this work, or allow others to do so, for U.S. Government purposes.

Dylan Wald is a graduate student at the Colorado School of Mines (dylanwald@mines.edu), Kathryn Johnson is a professor at the Colorado School of Mines (kjohnson@mines.edu), Christopher J. Bay is a research engineer at the National Renewable Energy Laboratory (NREL) (christopher.bay@nrel.gov), Jennifer King is a research engineer at NREL (jennifer.king@nrel.gov), and Rohit Chintala is a research engineer at NREL (rohit.chintala@nrel.gov. [1]Colorado School of Mines, Golden, CO 80401, USA. [2]NREL, Golden, CO 80401, USA.

reducing computational burdens. Additionally, distributed MPC (DMPC) can be a solution in larger systems [21], [22]. Reference [22] uses DMPC to optimally control a six-zone building to follow a temperature setpoint.

While the works of [12], [17]–[22] describe the benefits of building control, few consider the building's impact on the grid infrastructure or communication amongst diverse neighboring devices. The work in [23] leverages work in [24], specifically its use of MPC for building control. However, additional communication among heterogeneous devices (the EVs and building) is introduced in [23] to aid the grid.

While the results in [23] validate the importance of coordinated communication between subsystems, the communication is very subsystem-specific (non-generalized). This paper works to generalize the Network Lasso-ADMM - Limited Communication - DMPC (NALD) algorithm to both improve the performance of the algorithm, and to allow the possibility for plug-and-play capabilities across other unique controllable devices. The main contributions of this paper, compared to [23], include: 1) an altered objective function in the charging station subsystem, 2) an updated communication scheme, and 3) tuning the objective function weights and smoothing the control actions. These contributions lead to an overall improved performance of the NALD algorithm.

II. NALD Algorithm

In [23], the purpose of the NALD algorithm is to allow coordinated communication between two devices with different objectives achieve of both local and global objectives. The global objective is to

$$\text{minimize} \quad e^t = P^t_{ref} - P^t_{tot} \tag{1}$$

where P_{tot} is the total power including both the building and charging stations and P_{ref} is the power reference from the grid. In the NALD algorithm summarized in Fig. 1, the framework presented in [24] and [25] is used wherein each subsystem communicates only with its neighboring subsystems. Sections II-A – II-C explain the subsystems in Fig. 1. Note that the communication in Fig. 1 occurs a designated amount of times, or communication iterations, between each control time step.

A. Grid Aggregator Configuration

Identically to [23] and [24], the grid aggregator subsystem (left subsystem in Fig. 1) uses the limited-communication distributed model predictive control (LC-DMPC) framework described in [24] and [25]. In the NALD algorithm, the grid aggregator subsystem receives and distributes the bulk power reference signal P_{ref} from the grid. The subsystem's two objectives are to 1) follow the bulk reference signal from the grid and 2) ensure an appropriate power setpoint value P_{set} is communicated to the building. The grid aggregator must provide the building with a setpoint that is sufficient for the aggregate building and charging station subsystems' load. In Fig 1, the grid aggregator's objective function also includes a sensitivity term $\Psi_{ga} Z_{ga}$ (left subsystem, middle block). A sensitivity that is received from another subsystem is denoted as Ψ and a sensitivity that is communicated to other subsystems is denoted as γ. Using LC-DMPC, the grid aggregator optimizes its control action across a finite horizon, calculates a sensitivity γ_{ga}, and communicates this information each communication iteration, implementing the first step of the optimized control action each time step.

B. Building Configuration

The building subsystem also utilizes the LC-DMPC framework in [24] and [25]. In the NALD algorithm, the building subsystem aims to 1) track the power setpoint value from the grid aggregator P_{set} and 2) track the building's internal temperature reference T_m. Details of the building subsystem controller can be found in [23] and [24]. The building's objective function includes a sensitivity component $\Psi_b Z_b$, as shown in Fig. 1 (middle subsystem, middle block). Although using a weight matrix S with all 0 entries appears to decouple the control action U from the objective, U still impacts the output vector Y for indirect inclusion. The building optimizes its control action over a finite horizon using LC-DMPC, calculates a sensitivity γ_{ga}, and communicates this information each communication iteration, applying the first control action to the building model each time step. Like in [23] and [24], the building dynamics are approximated using a reduced-order 3-resistor, 2-capacitor (3R2C) model, developed from EnergyPlus [26] using an extended kallman filter (EKF) to estimate its parameters [27]. It is assumed that only the building's HVAC system is controllable and is the main source of power consumption. Hence, the internal temperature estimation from the 3R2C model is based on cooling provided by the HVAC system, as well as current weather conditions (generated from EnergyPlus [26]) and a small internal load (data based on building occupant schedules within a U.S. DOE large office building [28]).

C. Electric Vehicle Configuration

Like [23], the charging station subsystem in this work uses a hierarchical, consensus-based EV charging control logic. In this subsystem, there are N charging stations, each with n_i number of plugs, in which each plug in charging station $i \in N$ is represented as p where $p \in n_i$. Each charging station is connected via an undirected graph $\mathcal{G}$ with vertices and edges defined as $\mathcal{V}$ and $\mathcal{E}$, respectively [29]. Each charging station in set $\mathcal{V}$ communicates across its edges $\mathcal{E}$ to optimize each charging rate $x_{i,p}$ and come to consensus on their aggregate charging loads $\mathbf{x}_i$. The level of consensus is facilitated by the size of the regularization parameter λ; refer to [29] for details. Across this undirected network, the charging station subsystem uses its own distributed control logic to minimize the total EV charging load. The charging station objective function is of the form

$$\begin{aligned} \text{minimize} \quad & \underbrace{\sum_{i \in \mathcal{V}} f_i(\mathbf{x}_i)}_{\text{node objective}} + \underbrace{\sum_{(j,k) \in \mathcal{E}} g_{j,k}(\mathbf{x}_j, \mathbf{x}_k)}_{\text{edge objective}} \\ & i = 1, ..., N \quad j \in \mathcal{N}(i) \end{aligned} \tag{2}$$

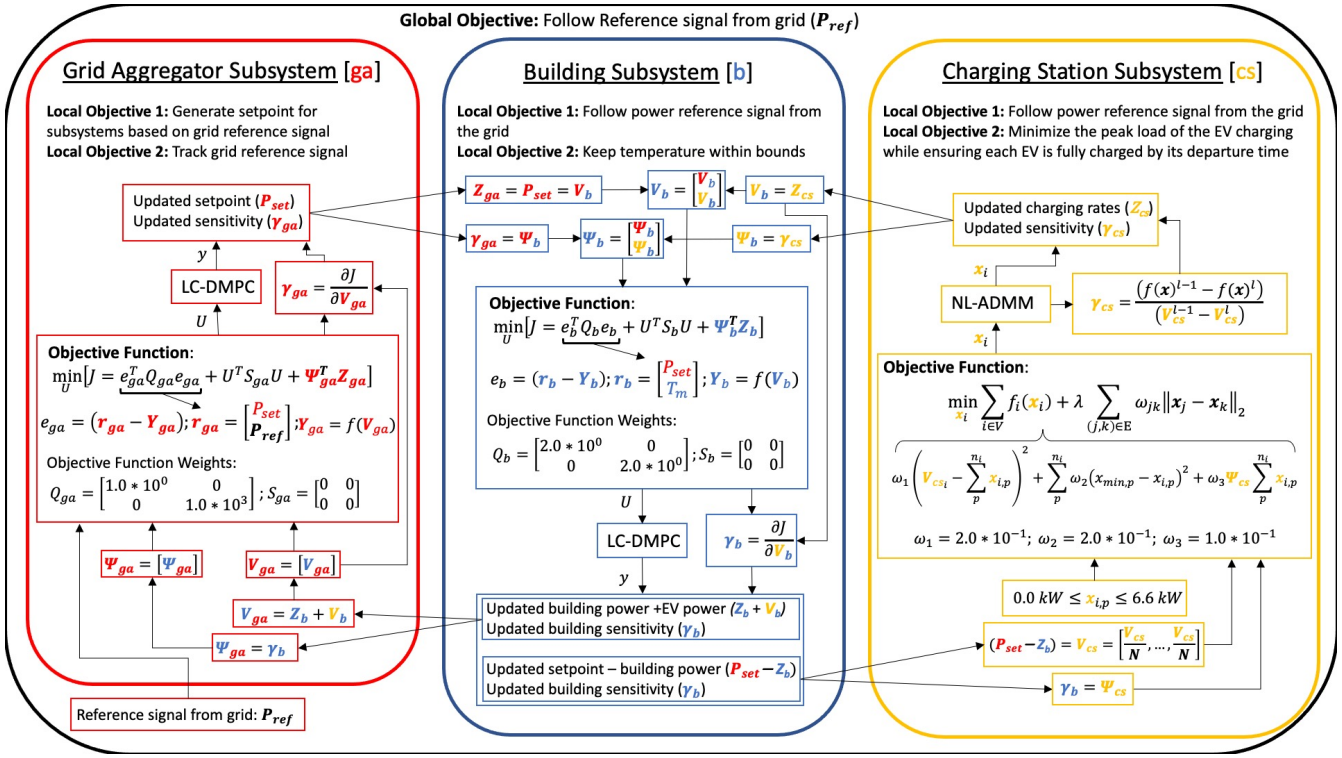

Fig. 1. Communication schematic of the NALD algorithm. The red (ga) represents the grid aggregator, the blue (b) represents the building, and the orange (cs) represents the charging stations. The arrows show the direction of communication during an iteration. Specific descriptions for the grid aggregator, building, and charging station subsystems can be found in Sections II-A, II-B, and II-C, respectively.

where the node objective $f_i(\cdot)$ is a cost function associated with node (charging station) i and the edge objective $g_{j,k}(\cdot,\cdot)$ is a cost function associated with edge (j,k) [29].

In the NALD algorithm developed in [23], the local node objective for the charging station subsystem was to minimize the peak load while keeping each EV charging rate within specified bounds to ensure a full charge, or

$$f_i(\mathbf{x}_i) = \underbrace{P_b + \sum_{p=0}^{n_i} x_{i,p}}_{\text{Power Component}} + \underbrace{c \sum_{z=0}^{n_{i,a}} \left(\frac{E_{i,a}}{x_{i,a}} \right)}_{\text{Time Component}} \quad \text{s.t.} \quad x_{min,p} \leq x_{i,p} \leq x_{max,p} \tag{3}$$

where P_b is the building power, $E_{i,a}$ the remaining energy each EV would need to consume to reach full charge, a is an active plug, and c is a weight on the time component. The reader is referred to [23] for details of each component. It was found that this typically imposed a narrow range of charging rate bounds, limiting the flexibility of the EV charging controller each iteration and thus its overall ability to contribute to the reference tracking.

We now define a new node objective function for the charging station subsystem that allows for increased flexibility. While the distributed, consensus-based control logic remains, the specific node objective function $f_i(\cdot)$ is slightly altered. In addition to the increased flexibility, the new node objective function is more similar to the other subsystems' objective functions. This similarity will enable each individual objective to be more easily tuned (refer to Section III). The new charging station node objective function is thus

$$f_i(\mathbf{x}_i) = \omega_1 \left((P_{set} - P_b) - \sum_{p=0}^{n_i} x_{i,p} \right)^2 + \sum_{p=0}^{n_i} \omega_2 \left(x_{min,p} - x_{i,p} \right)^2 + \omega_3 \Psi_{cs} \sum_{p=0}^{n_i} x_{i,p} \quad \text{s.t.} \quad 0.0 \leq x_{i,p} \leq x_{max} \tag{4}$$

where the first term is the (global) power setpoint tracking term, the second is the (local) minimum charge bound tracking term, and the third is the sensitivity term. From the bottom right of Fig. 1, $\Psi_{cs} = \gamma_b$. Here, Ψ_{cs} is used in the charging station subsystem's objective function to facilitate coordination.

Because the the charging station subsystem can only communicate with the grid subsystem indirectly through the building, it actually tracks the power difference $P_{set} - P_b$ instead of tracking P_{set}. In the second term of (4), the EV at each plug p in charging station i attempts to track its minimum charging rate $x_{min,p}$ at that time. This minimum charging rate refers to the minimum possible charging rate each EV can implement to be fully-charged by its departure time (updated at each time step). In this new objective function (4), the bounds described in [23] are removed, allowing each EV to optimize its charge rate over the full

charging range $0.0 < x_{i,p} < x_{max} = 6.6$ kW. This wider range allows the charging station controller to better support the grid. Last, note that since the charging station subsystem does not use MPC, it communicates an array of constant signals across the finite horizon to the building subsystem.

III. COORDINATION THROUGH SENSITIVITY

In Fig. 1, the building and grid aggregator subsystems calculate their sensitivities γ_b and γ_{ga} according to

$$\gamma = \frac{\partial J}{\partial V} \tag{5}$$

where in each case J is their objective function and V is their incoming disturbance from their neighbor (s). In this work, the charging station subsystem's sensitivity γ_{cs} is calculated similarly to facilitate improved subsystem coordination to prior work [23]. The charging station sensitivity γ_{cs} is calculated using

$$\gamma_{cs} = \frac{f(\mathbf{x}_i)^{l-1} - f(\mathbf{x}_i)^{l}}{V_{cs}^{l-1} - V_{cs}^{l}} = \frac{\Delta f(\mathbf{x}_i)}{\Delta V} \tag{6}$$

where $f(\mathbf{x}_i)$ is the node objective function, V_{cs} is the incoming disturbance from the building P_b, and l is the iteration number. The meaning of this discrete sensitivity calculation — as read by the building subsystem — can be reflected in four different cases, providing a framework for cooperative communication between the subsystems. Table I summarizes these four cases.

TABLE I
CHARGING STATION SUBSYSTEM SENSITIVITY CASES AND INTERPRETATIONS
cont. = continues

Case	Characteristics of (6)	Interpretation
1	$\Delta f(\mathbf{x}_i) > 0; \Delta V < 0$	P_b keeps $\uparrow$ so $f(\mathbf{x}_i)$ cont. to $\downarrow$
2	$\Delta f(\mathbf{x}_i) < 0; \Delta V > 0$	P_b starts to $\uparrow$ to help $\downarrow f(\mathbf{x}_i)$
3	$\Delta f(\mathbf{x}_i) > 0; \Delta V > 0$	P_b keeps $\downarrow$ so $f(\mathbf{x}_i)$ cont. to $\downarrow$
4	$\Delta f(\mathbf{x}_i) < 0; \Delta V < 0$	P_b starts to $\downarrow$ to help $\downarrow f(\mathbf{x}_i)$

A. Optimal Weighting

In order to achieve the best algorithm performance, the weights in each subsystem's objective function must be appropriately tuned. Within the NALD algorithm, there are seven different adjustable weights: the grid aggregator subsystem objective function weights Q_{ga_1} and Q_{ga_2}, the building subsystem objective function weights Q_{b_1} and Q_{b_2}, and the charging station subsystem objective function weights ω_1, ω_2, and ω_3. In this work, weights $Q_{ga_1} = 1000$, $Q_{ga_2} = 1.0$, $Q_{b_1} = 2.0$, and $Q_{b_2} = 2.0$ are held constant. These values were selected based on simulation experiments and can be modified to achieve user preference. We then manually tuned ω_1, ω_2, and ω_3 in the charging station subsystem. We plot their performance in terms of the normalized (by its maximum value) mean average error (MAE) and normalized root mean square error (RMSE) for each subsystem compared to the sum of their local and global references. We then determine the total error magnitude by adding each normalized tracking error for each scenario. The results are shown in Fig. 2.

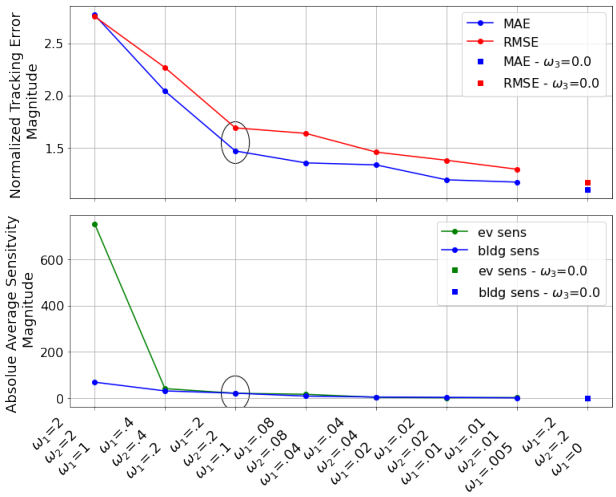

Fig. 2. **Top:** Normalized tracking error magnitude at each weight scenario. The y-axis represents the sum of the normalized tracking errors (three values each normalized to [0, 1] and then added) and the x-axis indicates the charging station weights used for each test case (same as the x-axis in the bottom plot). **Bottom:** Mean absolute building and charging station sensitivity values. The sensitivity magnitudes are almost the same in the third scenario. The black circles represent the results associated with the weights selected and the square markers represent the scenarios with $\omega_3 = 0.0$.

In Fig. 2, $\omega_1 = \omega_2$ and $\omega_3 = \frac{1}{2}\omega_1$ in all cases except the last. From the base case to a factor of 10 decrease in weight values, the normalized error magnitudes (MAE and RMSE) decrease significantly. Notice a slight point of inflection at weights $\omega_1 = 0.2, \omega_2 = 0.2, \omega_3 = 0.1$, indicated as the circled point in the top plot. At these weights, the sensitivity values have nearly the same average absolute magnitude as shown in the bottom plot of Fig. 2, meaning that the sensitivities of each subsystem will carry approximately the same weight in the overall optimization to facilitate subsystem coordination and tuning. For these reasons, these weights were chosen as the most beneficial and will be used for the remainder of this paper. If $\omega_3 = 0.0$, the optimization does not depend on the charging station's sensitivity and the error is the lowest across all of the weight choices shown for the scenario studied. However, this weight scheme is not chosen for reasons described in Section IV-C.

B. Smoothing

With objective function weights Q and ω properly tuned, the power and sensitivity signals from each subsystem are still very noisy, resulting in errors greater than desired. To alleviate this issue, we implement each subsystem's control signal U via

$$U^l = \beta U^{l-1} + (1-\beta) U_{QP}^l \tag{7}$$

where l is the communication iteration number, U_{QP}^l is the optimal control action determined by each objective function at iteration l, and β is the tunable convex combination

parameter that filters high frequency control changes. This β smooths out the trajectory of each subsystem's actions. Note that the LC-DMPC algorithm in [25] already includes (7), while the charging station subystem in [23] does not. Hence, in [23], $\beta = 0.1$ for the grid aggregator and building subsystems. The filter (7) is now applied to all subsystems and the algorithm performance using different values of β is shown in Fig. 3.

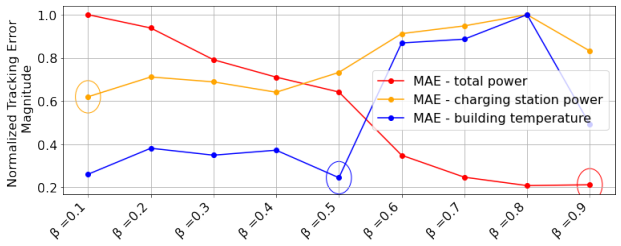

Fig. 3. Normalized MAE for each objective across different values of β. There are different minima in the normalized error magnitudes for each objective depicted by the appropriately colored circles.

Fig. 3 shows that each of the three error measures are minimized at a different value of β: $\beta = 0.9$ for the power reference tracking error, $\beta = 0.1$ for the minimum charge bound error, and $\beta = 0.5$ for the temperature tracking error. Thus, selecting β depends on operator priorities regarding which error is most important.

To further investigate the effect of (7) on the performance of the NALD algorithm, we define a smoothness metric S_ϕ to determine the noisiness of a signal as

$$S_\phi = \|(\phi^m - \phi^{m-1})\|_2 \tag{8}$$

where ϕ represents the signal of interest and m represents each discrete time step in ϕ. Equation (8) is the ℓ_2-norm on ϕ. As S_ϕ is larger, the signal is more noisy and vice versa.

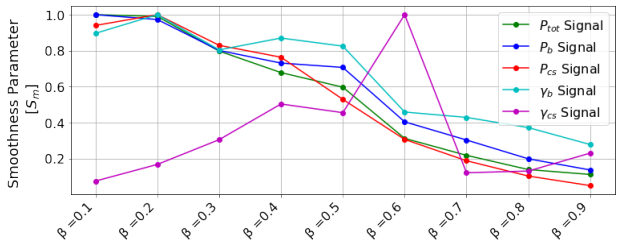

Fig. 4. Measure of smoothness for each signal (total power P_{tot}, building power P_b, charging station power P_{cs}, building sensitivity γ_b, and charging station sensitivity γ_{cs} signals) across different values of β.

Fig. 4 plots the smoothness of five separate signals, which is normalized to aid visualization of the trends. Each signal in Fig. 4, apart from the charging station sensitivity signal, increases in smoothness as β increases where $\beta = 0.9$ generally results in the smoothest signal. When considering results in Fig. 3 and 4, we use $\beta = 0.9$ for the remainder of this paper.

IV. RESULTS AND DISCUSSION

A. Simulation Setup

We now establish the simulation environment. First, the grid aggregator receives an arbitrary six-hour power reference signal P_{ref} initially centered at 80 kW with a start time of 08:20, increased to 110 kW at 10:50, and finally decreased to 60 kW at 12:30. This signal includes some normally distributed random fluctuations from the mean values. Like in [23], real weather conditions, including outdoor temperature and solar irradiance as well as an estimated internal load profile, are applied to the building model ([26], [28]). For the charging station subsystem, three charging stations are used with 8, 10, and 9 plugs in each. Up to three charging events on each plug are allowed per day, but not all plugs experience three events, resulting a total of 43 total events. The EV events are randomly chosen from a large dataset generated by the software in [30]. Six communication iterations between control time steps of one minute are used. A MPC horizon length of three minutes is used.

B. Simulation Results

To illustrate the performance of the NALD algorithm, we plot a time series of each tracking term in Fig. 5. The building internal temperature tracking is shown in the top plot, followed by the minimum charging rate bound $x_{min,p}$ tracking in the middle plot, and finally, the total power reference tracking in the bottom plot.

As discussed in Section II, the NALD algorithm contains two local subsystem objectives and one global objective. The top plot of Fig. 5 shows that the temperature profile is very smooth and remains within $1.24°C$ of the reference temperature. The oscillations in the temperature profile are due to the sharp changes in the power reference signal, changes in individual subsystem power consumption, and in some cases, the constant increase in outdoor temperature. The latter two effects can be seen near 09:10. Here, the charging station initially consumes less power, which means that to track the power setpoint the building must consume more power. However, as time progresses, the charging station begins consuming more power, so the building begins consuming less. This, along with a steady increase in the outdoor temperature, causes the rise in building temperature in the top plot of Fig. 5. In addition to the excellent tracking of the internal building temperature, the temperature stays within the thermal comfort bounds, successfully fulfilling the building subsystem's local objective.

Recall from Section II-C that the charging station subsystem's local objective is to minimize the difference from the charging rate $x_{i,p}$ of each EV at plug p in charging station i from its corresponding minimum charge rate $x_{min,p}$. The middle plot in Fig. 5 shows that the aggregate charging station load somewhat follows the minimum charge bound. It is relatively smooth, but has some lag in its response between 08:20 – 10:00. This lag is due to the phase lag on the control action from the large β value along with the selected initial conditions. It is important for the aggregate charging load

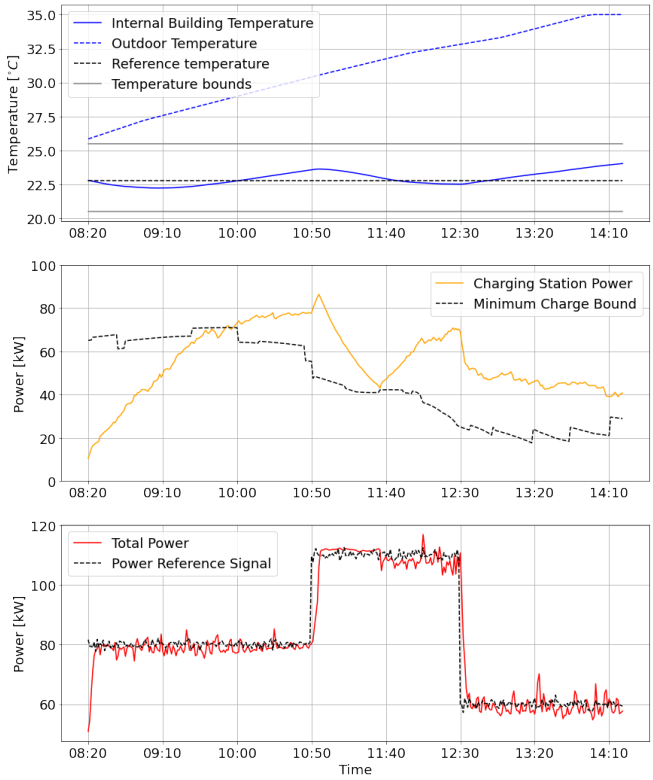

Fig. 5. **Top:** Temperature tracking within the building subsystem. The two grey lines show the temperature bounds, the dashed black line shows the reference temperature, and the blue line shows the actual building internal temperature. **Middle:** Minimum charging rate bound tracking. The black dashed line represents the aggregate minimum charging rate of each EV and the orange line represents the actual aggregate charging rate of each EV. **Bottom:** Total power reference tracking of the NALD algorithm. The black dashed line shows the power reference signal P_{ref} and the red line shows the total power consumed by both the building and charging stations.

to follow the minimum charge bound both to minimize the overall charging load and to allow the EVs to fully charge by their departure times $t_{d,p}$. In this work, we do not quantify whether each EV is fully charged by its departure time because the simulation occurs during a partial day, i.e., some charging events have not reached their departure time when the simulation ends. However, total energy consumed by the EVs is more than 120% of the energy required to meet the minimum charge bound. From this calculation, we deduce that the EVs consume enough energy to at least get near full charge by their departure times.

The global objective of the NALD algorithm is to provide ancillary services to the grid by following an allotted power reference signal. The bottom plot in Fig. 5 shows the power reference tracking performance of the NALD algorithm for this specific scenario. After an initial spike due to initial conditions, the total power signal in the bottom plot of Fig. 5 follows the reference signal extremely well. In fact, the MAE for the entire time series is less than 3 kW (2.92 kW).

C. Importance of the Charging Station Sensitivity Term

While it may not appear optimal to include non-zero ω_3, in terms of the results shown in Fig. 2 and Fig. 5, it proves to be critical in other scenarios. Fig. 6 shows the

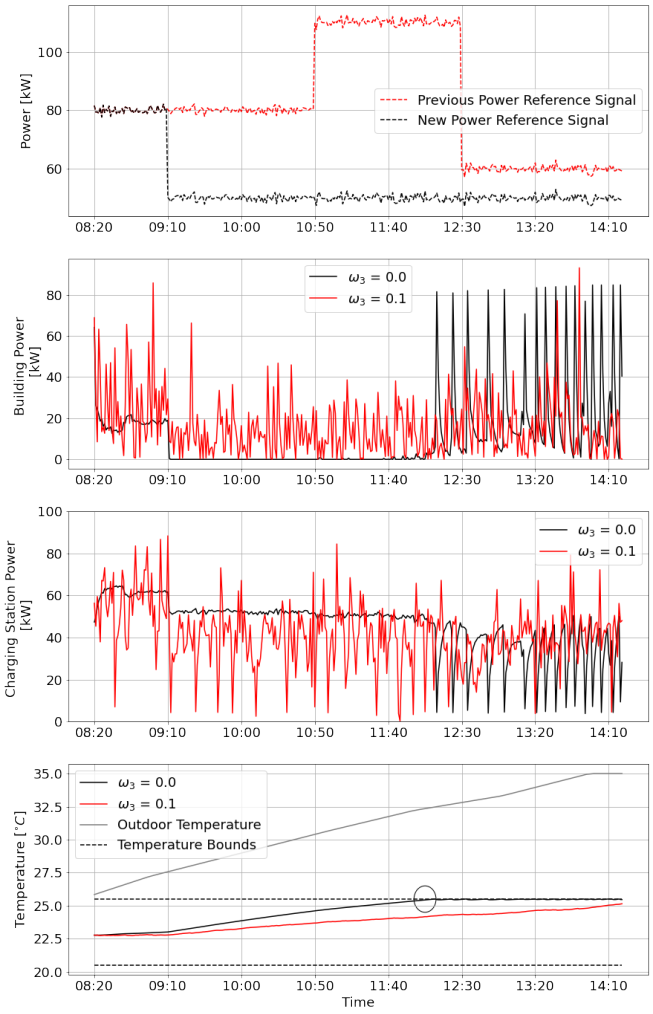

Fig. 6. **Top:** New power reference signal used compared to the signal used to produce the Section IV-B results. **Second Plot:** Power consumed by the building. **Third Plot:** Power consumed by the EVs. **Bottom:** Internal temperature of the building as well as the outdoor temperature, including the upper and lower temperature bounds. Note that each plot shows the response for cases $\omega_3 = 0.1$ (black) and $\omega_3 = 0.0$ (red). The temperature violation is marked by the black circle.

building and charging station power usage along with the building temperature for the same six-hour period described in Section IV-B. However, we include another, much smaller power reference signal, as shown in the top plot in Fig. 6. When the charging station subsystem does not account for the building's sensitivity ($\omega_3 = 0.0$) any sort of coordination is removed. This lack of coordination causes the building to violate its upper temperature bound, as depicted by the solid black line in the bottom plot of Fig. 6. Conversely, if $\omega_3 = 0.1$, the charging station can see the needs of the building and thus coordinates. This coordination slightly worsens the minimum charge bound tracking of the charging station subsystem, but improves the temperature tracking of the building. Hence, $\omega_3 = 0.0$ decreases the robustness of the NALD algorithm in more difficult cases such as the one shown from Fig. 6. Note that with $\omega_3 > 0$, the power signal shown in the middle plot of Fig. 6 is much noisier than in Fig. 5. This is a matter of scaling and smoothing and is

something that will be investigated in future work.

V. CONCLUSIONS

As more controllable devices are introduced onto the grid, their ability to provide services to the grid is limited by their individual needs and capabilities. If these devices communicate in a cooperative manner, they have the ability to provide ancillary services to the grid while continuing to perform optimally. The NALD algorithm provides a framework to do just that, even with a diverse set of subsystems. While the NALD algorithm previously proved to perform well in a unique scenario [23], this work takes a step toward further generalizing the algorithm. By altering the objective function in the charging station subsystem designed in prior work to resemble the LC-DMPC objective function, the charging station's sensitivity value can be calculated in a way that is similar to and thus better understood by other subsystems in the LC-DMPC framework. With proper weighting and smoothing parameters applied, the updated NALD algorithm yields a much improved performance compared to [23].

While these improvements take a step towards a generalized method for coordinated communication between controllable devices, additional opportunities for improvement remain. Future work involves further generalizing the NALD algorithm by normalizing its objectives and variables. Additionally, as an attempt to move toward real-world implementation, real reference signals will be explored, including real-world performance criteria. Last, as the NALD algorithm becomes more generalized, other controllable devices (in addition to buildings and EVs) will be explored and implemented into the framework.

REFERENCES

[1] B. D. Kroposki, E. Dall-Anese, A. Bernstein, Y. Zhang, and B. S. Hodge, "Autonomous energy grids," National Renewable Energy Laboratory, Golden, CO (United States), Tech. Rep., 2017.

[2] X. Zhou, Z. Liu, W. Wang, C. Zhao, F. Ding, and L. Chen, "Hierarchical distributed voltage regulation in networked autonomous grids," in *American Control Conf.*, 2019, pp. 5563–5569.

[3] J. Cochran, M. Miller, O. Zinaman, M. Milligan, D. Arent, B. Palmintier, M. O'Malley, S. Mueller, E. Lannoye, A. Tuohy, B. Kujala, M. Sommer, H. Holttinen, J. Kiviluoma, and S. Soonee, "Flexibility in 21st century power systems," National Renewable Energy Laboratory, Golden, CO (United States), Tech. Rep., 2014.

[4] C. McKerracher, A. Izadi-Najafabadi, A. O'Donovan, N. Albanese, N. Soulopolous, D. Doherty, M. Boers, R. Fisher, C. Cantor, J. Frith, S. Mi, and A. Grant, "Electric vehicle outlook 2020," BloombergNEF, Tech. Rep., 2020.

[5] K. Dayem, C. Mercier, and P. May-Ostendorp, "Electric vehicle charging control strategies," National Rural Electric Cooperative Association's Business and Technology Strategies dept., Tech. Rep., 2019.

[6] Z. Ma, D. S. Callaway, and I. A. Hiskens, "Decentralized charging control of large populations of plug-in electric vehicles," *IEEE Trans. on Control Systems Technology*, vol. 21, no. 1, pp. 67–78, 2013.

[7] M. Liu, P. K. Phanivong, Y. Shi, and D. S. Callaway, "Decentralized charging control of electric vehicles in residential distribution networks," *IEEE Trans. on Control Systems Technology*, vol. 27, no. 1, pp. 266–281, 2019.

[8] A. Di Giorgio, F. Liberati, and S. Canale, "Electric vehicles charging control in a smart grid: A model predictive control approach," *Control Engineering Practice*, vol. 22, pp. 147–162, 2014.

[9] M. A. López, S. De La Torre, S. Martín, and J. A. Aguado, "Demand-side management in smart grid operation considering electric vehicles load shifting and vehicle-to-grid support," *Int. Journal of Electrical Power & Energy Systems*, vol. 64, pp. 689–698, 2015.

[10] D. Wu, N. Radhakrishnan, and S. Huang, "A hierarchical charging control of plug-in electric vehicles with simple flexibility model," *Applied Energy*, vol. 253, p. 113490, 2019.

[11] S. Baldwin *et al.*, "Quadrennial technology review: an assessment of energy technologies and research opportunities," U.S. DOE, Tech. Rep., 2015.

[12] A. Afram and F. Janabi-Sharifi, "Theory and applications of HVAC control systems–a review of model predictive control (mpc)," *Building and Environment*, vol. 72, pp. 343–355, 2014.

[13] J. Drgoňa and M. Kvasnica, "Comparison of MPC strategies for building control," in *Int. Conf. on Process Control*, 2013, pp. 401–406.

[14] F. Oldewurtel, A. Ulbig, A. Parisio, G. Andersson, and M. Morari, "Reducing peak electricity demand in building climate control using real-time pricing and model predictive control," in *49th IEEE Conf. on Decision and Control*, 2010, pp. 1927–1932.

[15] A. Martinčević, M. Vašak, and V. Lešić, "Model predictive control for energy-saving and comfortable temperature control in buildings," in *24th Mediterranean Conf. on Control and Automation*, 2016, pp. 298–303.

[16] F. Oldewurtel, A. Parisio, C. N. Jones, D. Gyalistras, M. Gwerder, V. Stauch, B. Lehmann, and M. Morari, "Use of model predictive control and weather forecasts for energy efficient building climate control," *Energy and Buildings*, vol. 45, pp. 15–27, 2012. [Online]. Available: https://www.sciencedirect.com/science/article/pii/S0378778811004105

[17] C. J. Bay, R. Chintala, and B. P. Rasmussen, "Steady-state predictive optimal control of integrated building energy systems using a mixed economic and occupant comfort focused objective function," *Energies*, vol. 13, no. 11, p. 2922, 2020.

[18] R. Jia, M. Jin, K. Sun, T. Hong, and C. Spanos, "Advanced building control via deep reinforcement learning," *Energy Procedia*, vol. 158, pp. 6158–6163, 2019.

[19] S. Yang, M. P. Wan, W. Chen, B. F. Ng, and S. Dubey, "Experiment study of machine-learning-based approximate model predictive control for energy-efficient building control," *Applied Energy*, vol. 288, p. 116648, 2021.

[20] ——, "Model predictive control with adaptive machine-learning-based model for building energy efficiency and comfort optimization," *Applied Energy*, vol. 271, p. 115147, 2020.

[21] E. Camponogara, D. Jia, B. Krogh, and S. Talukdar, "Distributed model predictive control," *IEEE Control Systems Magazine*, vol. 22, no. 1, pp. 44–52, 2002.

[22] R. Eini and S. Abdelwahed, "Distributed model predictive control based on goal coordination for multi-zone building temperature control," in *IEEE Green Technologies Conf.*, 2019, pp. 1–6.

[23] D. Wald, J. King, C. J. Bay, R. Chintala, and K. Johnson, "Integration of distributed controllers: Power reference tracking through charging station and building coordination," *Applied Energy*, vol. 314, p. 118753, 2022. [Online]. Available: https://www.sciencedirect.com/science/article/pii/S0306261922002070

[24] C. J. Bay, R. Chintala, V. Chinde, and J. King, "Distributed model predictive control for coordinated, grid-interactive buildings," *Applied Energy*, vol. 312, p. 118612, 2022. [Online]. Available: https://www.sciencedirect.com/science/article/pii/S0306261922000861

[25] R. E. Jalal and B. P. Rasmussen, "Limited-communication distributed model predictive control for coupled and constrained subsystems," *IEEE Trans. on Control Systems Technology*, vol. 25, no. 5, pp. 1807–1815, 2017.

[26] U.S. Department of Energy, "Energyplus simulation software version 9.5.0," 2020. [Online]. Available: https://www.energycodes.gov/prototype-building-models#Commercial

[27] R. Chintala, J. Winkler, and X. Jin, "Automated fault detection of residential air-conditioning systems using thermostat drive cycles," *Energy and Buildings*, vol. 236, p. 110691, 2021. [Online]. Available: https://www.sciencedirect.com/science/article/pii/S0378778820334770

[28] U.S. Department of Energy, "Commercial prototype buildings," 2021. [Online]. Available: https://www.energycodes.gov/prototype-building-models#Commercial

[29] D. Hallac, J. Leskovec, and S. Boyd, "Network lasso: Clustering and optimization in large graphs," in *Proc. of the 21th ACM SIGKDD int. conf. on knowledge discovery and data mining*, 2015, pp. 387–396.

[30] E. W. Wood, C. L. Rames, and M. Muratori, "New EVSE analytical tools/models: Electric vehicle infrastructure projection tool (evi-pro)," 2018. [Online]. Available: https://www.osti.gov/biblio/1419413